nature cell biology

ARTICLES

https://doi.org/10.1038/s41556-018-0216-y

Pancreatic islet-autonomous insulin and smoothened-mediated signalling modulate identity changes of glucagon$^+$ α-cells

Valentina Cigliola[1,2,10], Luiza Ghila[1,3,10], Fabrizio Thorel[1,10], Léon van Gurp[1], Delphine Baronnier[1], Daniel Oropeza[1], Simone Gupta[4], Takeshi Miyatsuka[5], Hideaki Kaneto[6], Mark A. Magnuson[7], Anna B. Osipovich[7], Maike Sander[8], Christopher E. V. Wright[9], Melissa K. Thomas[4], Kenichiro Furuyama[1], Simona Chera[1,3] and Pedro L. Herrera[1*]

The mechanisms that restrict regeneration and maintain cell identity following injury are poorly characterized in higher vertebrates. Following β-cell loss, 1–2% of the glucagon-producing α-cells spontaneously engage in insulin production in mice. Here we explore the mechanisms inhibiting α-cell plasticity. We show that adaptive α-cell identity changes are constrained by intra-islet insulin- and Smoothened-mediated signalling, among others. The combination of β-cell loss or insulin-signalling inhibition, with Smoothened inactivation in α- or δ-cells, stimulates insulin production in more α-cells. These findings suggest that the removal of constitutive 'brake signals' is crucial to neutralize the refractoriness to adaptive cell-fate changes. It appears that the maintenance of cell identity is an active process mediated by repressive signals, which are released by neighbouring cells and curb an intrinsic trend of differentiated cells to change.

Half a century of research into cell identity determination and maintenance has revealed that adult cells are not terminally differentiated but maintain some plasticity potential even in higher organisms[1–3]. Spontaneous adult cell-type interconversion is considered a rare event that is highly regulated, often activated exclusively after injury and whose efficiency correlates with mechanisms preserving a specific cell identity[2,4]. Conversely, our knowledge of the intricate mechanisms that maintain adult cell identity is still limited.

Cell-fate allocation and maintenance[1,5,6] result from the activity of transcriptional regulators and epigenetic modifiers that control the constitutive expression of identity genes that become 'locked' due to autoregulatory feed-back loops, stable chromatin modifications[7–9] or through the action of regulatory signals from the micro-environment in which cells reside. The plasticity potential of a given cell depends on the level of redundancy in which these complex mechanisms operate and on the physiological needs of the corresponding tissue.

Changes in adult cell identity, especially if triggered by stress responses, are a basis for in situ regenerative medicine[10,11]. In the pancreas of adult mice, following near-total β-cell ablation, 1–2% of glucagon-expressing α-cells and somatostatin-expressing δ-cells spontaneously express insulin, leading to significant β-cell mass regeneration and normoglycaemia[12,13]. The mechanisms controlling this insulin expression are unknown. We have previously shown that in α-cells, inhibition of the transcription factor Arx and the dimethyltransferase Dnmt1 causes transdifferentiation into insulin$^+$ cells irrespective of β-cell loss[14]. However, nothing is known about the control of α-cell identity by extrinsic signals. Here we define the cellular mechanisms that regulate the expression of insulin in glucagon$^+$ α-cells after near-total β-cell ablation or insulin action inhibition. We focus on local signals that act as constitutive brakes that limit cell reprogramming. We identified Smoothened- and insulin-signalling pathways in α-cells, and surprisingly also in δ-cells, as regulators of α-cell identity and conversion into insulin-producing cells.

Results

Conversion of α-cells is driven by local signals. To elucidate the signals that lead to insulin production in α-cells following β-cell loss in mice, we set up a series of islet transplantation experiments (Fig. 1a). To prevent allograft rejection, we used severe combined immunodeficient (SCID) mice[15] as hosts for islets isolated from immunocompetent donor mice. In different experimental conditions, islet donor and/or recipient mice also bore the RIP-DTR transgene, which allowed for β-cell ablation following diphtheria toxin administration in either engrafted or pancreatic islets, or both[13]. As a readout for α-cell conversion to insulin production, we assessed the percentage of α-cells that co-expressed glucagon and insulin in the engrafted and/or pancreatic islets of the host. Indeed, cell lineage tracing experiments have shown that these bihormonal cells appearing after β-cell loss are reprogrammed α-cells[13].

[1]Department of Genetic Medicine and Development, iGE3 and Centre facultaire du diabète, Faculty of Medicine, University of Geneva, Geneva, Switzerland. [2]Present address: Department of Cell Biology, Duke University Medical Center, Durham, NC, USA. [3]Department of Clinical Science and KG Jebsen Center for Diabetes Research, University of Bergen, Bergen, Norway. [4]Lilly Research Laboratories, Lilly Corporate Center, Indianapolis, IN, USA. [5]Department of Metabolism and Endocrinology, Graduate School of Medicine , Juntendo University , Tokyo, Japan. [6]Department of Metabolic Medicine, Graduate School of Medicine, Osaka University, Osaka, Japan. [7]Departments of Molecular Physiology and Biophysics, Center for Stem Cell Biology, Vanderbilt University, Nashville, TN, USA. [8]Department of Pediatrics and Cellular and Molecular Medicine, University of California, San Diego, CA, USA. [9]Department of Cell and Developmental Biology, Program in Developmental Biology and Center for Stem Cell Biology, Vanderbilt University School of Medicine, Nashville, TN, USA. [10]These authors contributed equally: Valentina Cigliola, Luiza Ghila, Fabrizio Thorel. *e-mail: pedro.herrera@unige.ch

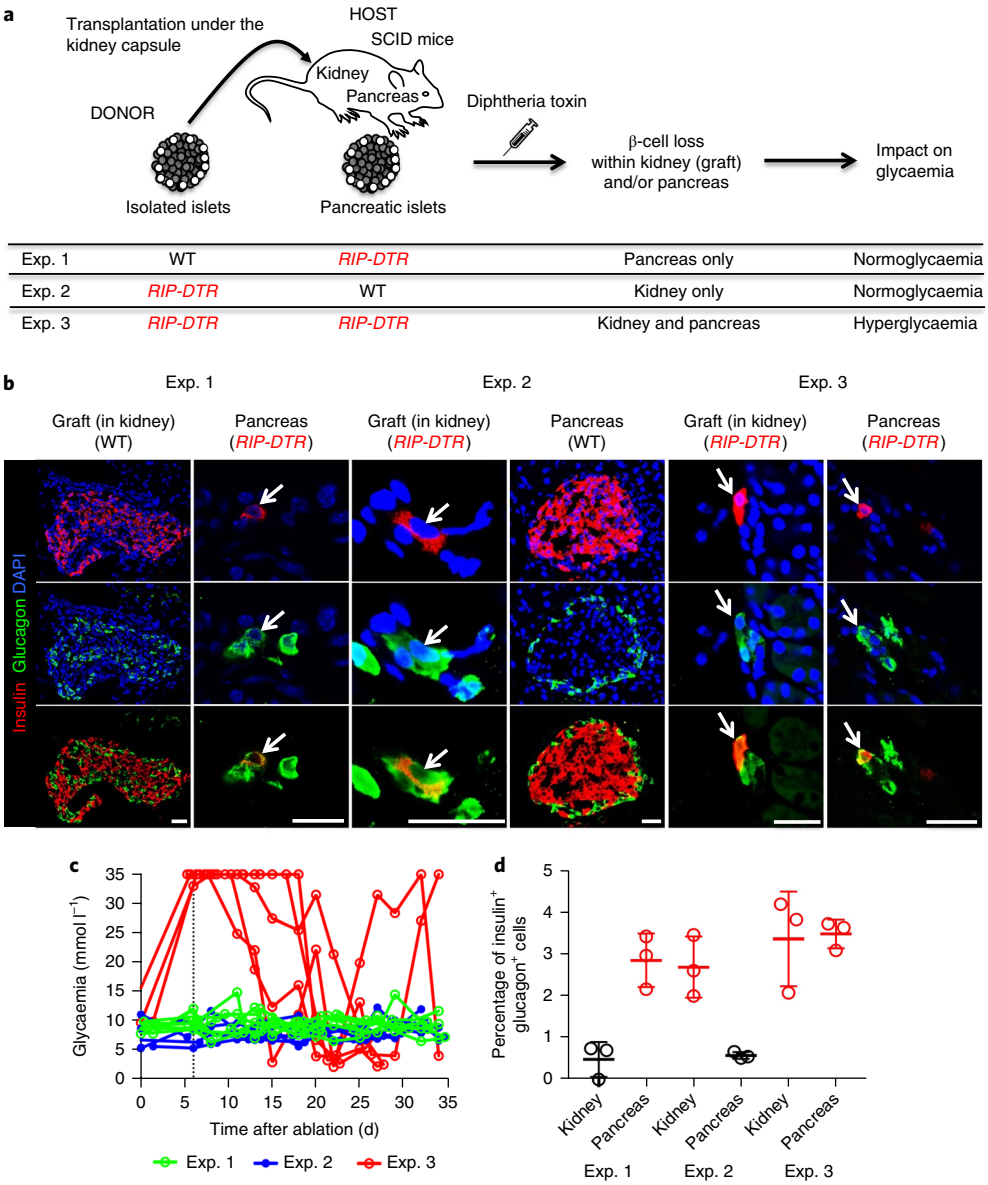

Fig. 1 | Insulin production engaged by α-cells after β-cell ablation in islets transplanted under the kidney capsule. a, Experimental design of islet transplantation underneath the kidney capsule of immunocompromised host mice (SCID). In Exp. 1, WT islets are transplanted into *RIP-DTR* hosts; following diphtheria toxin administration, β-cell ablation occurs in pancreatic islets, whereas transplanted islets remain unaffected and maintain normoglycaemia. In Exp. 2 and 3, islets isolated from *RIP-DTR* donors are transplanted into either WT or *RIP-DTR* hosts; diphtheria toxin only ablates β-cells in the transplanted islets (in WT hosts) or in both transplanted and endogenous pancreatic islets (in *RIP-DTR* hosts). **b**, Immunofluorescence staining of insulin (red) and glucagon (green) in Exps 1–3. The arrows indicate bihormonal glucagon$^+$insulin$^+$ cells. Scale bars, 20 μm. The experiment was repeated independently three times. **c**, Random-fed blood glycaemia after diphtheria toxin treatment in the three experimental conditions tested. The vertical dashed line indicates the administration of one insulin pellet to the hyperglycaemic mice. The experiment was performed once. **d**, Proportion of glucagon$^+$ cells co-expressing insulin. Red, *RIP-DTR* islets; black, WT islets; $n = 3$ biologically independent animals per condition. Data shown as mean ± s.d.; see Supplementary Table 1 for the source data.

We first transferred wild type (WT) islets (~700) under the kidney capsule of *RIP-DTR* SCID hosts to ensure normoglycaemia after diphtheria toxin-induced pancreatic β-cell loss (Fig. 1a, Experiment 1 (Exp. 1)). The reverse experiment, in which *RIP-DTR* islets were transferred into WT normoglycaemic *SCID* host mice, was also performed (Fig. 1a, Exp. 2). Ten days post-diphtheria toxin administration, β-cells were efficiently ablated in engrafted *RIP-DTR* islets (Supplementary Fig. 1a). We also transplanted islets from *RIP-DTR* mice into *RIP-DTR* SCID hosts (Fig. 1a, Exp. 3). In this experiment, diphtheria toxin treatment led to hyperglycaemia because of β-cell loss in both host and grafted islets (Fig. 1c, red lines). One month after β-cell ablation, insulin production in α-cells was observed in all three experiments, but only in β-cell-ablated islets (Fig. 1b,d), irrespective of their location (pancreatic or extra-pancreatic; Supplementary Table 1a) and glycaemia. Conversion of α-cells was also observed after β-cell ablation in *RIP-DTR* islets engrafted on the iris (anterior chamber of the eye) of normoglycaemic WT mice (not shown).

The percentage of α-cells producing insulin in β-cell-ablated islets (regardless of their location) was two-fold higher in *RIP-DTR*

SCID mice (1–2% versus 3–4% in SCIDs; refs [12,13]). This suggests that the genetic background (SCID) influences α-cell plasticity.

To explore the effect of global 50% β-cell mass loss, we co-transplanted WT and *RIP-DTR* islets at a 1:1 ratio into WT SCID hosts, either at two separate locations or mixed together at a single location (Supplementary Fig. 1b, Exp. 4). To distinguish the two types of engrafted islets, we labelled α-cells with yellow fluorescent protein (YFP) in *RIP-DTR* islets (using *Glucagon-rtTA*; *TetO-Cre*; *R26-YFP*; *RIP-DTR* mice as donors, in which doxycycline (DOX) triggers the irreversible expression of YFP in α-cells[13]) and β-cells with mCherry in WT islets (using islets from *Insulin-mCherry* mice, whose insulin-producing cells constitutively express mCherry). In the two-spot transplantation experiment, after diphtheria toxin treatment, no glucagon$^+$ cell was insulin$^+$ in unablated WT mCherry$^+$ islets, whereas 4% of YFP$^+$ α-cells produced insulin in β-cell-ablated *RIP-DTR* (Supplementary Fig. 1c and Supplementary Table 1a, Exp. 4). This further confirms that α-cells start insulin expression only in massively ablated islets. Similarly, no evidence of α-cell conversion after diphtheria toxin-mediated β-cell ablation was found in WT islets when mixed with *RIP-DTR* islets, whereas the proportion of YFP-labelled α-cells producing insulin in *RIP-DTR* islets was similar to the two-spot experiment (Supplementary Fig. 1c–d; Supplementary Table 1a, Exp. 4). This suggests that no signals act locally between adjacent β-cell-ablated (*RIP-DTR*) and unablated (WT) islets, neither from β-cell-ablated *RIP-DTR* islets that would promote conversion in WT islets with an intact β-cell mass nor from WT islets that would restrict α-cell conversion in nearby *RIP-DTR* islets.

We next explored the effect of 50% β-cell ablation occurring in every individual islet, either in the pancreas or after transplantation. We used hemizygous *RIP-DTR* females, in which about 50% of the β-cells express DTR[13]. In these settings (Exp. 5, Supplementary Table 1a), mice remained normoglycaemic after diphtheria toxin treatment and no evidence of α-cell conversion was observed (Supplementary Table 1a). Partial β-cell loss is thus insufficient to trigger α-cell conversion, even in the more permissive genetic backgrounds (that is, SCID mice).

In summary, these experiments reveal that α-cell conversion occurs only in islets undergoing massive β-cell loss, in an autonomous manner, irrespective of their location or glycaemia. The existence of signals from a putative systemic 'β-cell mass sensor' (Exps. 1–3) or acting at short distance (Exp. 4) is not supported, given that bihormonal cells were only detected in massively β-cell-ablated islets, in hyper- and normoglycaemic mice, and not in islets retaining approximately 50% of their β-cell mass (Exp. 5). Instead, our findings suggest that massive β-cell injury may lead to the release of local signals acting as modulators of α-cell change or maintenance.

Loss of β-cells facilitates insulin expression in α-cells. Why do most α-cells not express insulin after massive β-cell loss? To explore whether all α-cells can produce insulin, we induced Pdx1 (a β-cell-specific transcription factor) in αPdx1OE mice. In this quintuple transgenic line (Fig. 2a), the administration of DOX causes irreversible expression of Pdx1 and YFP in α-cells (Fig. 2b). The in vivo activity of Pdx1 in α-cells leads to the suppression of glucagon[16] (Fig. 2c–e and Supplementary Table 1b,c) and to insulin expression in a small subset (3%) of α-cells (Supplementary Table 1d). Yet most Pdx1-expressing α-cells produce insulin after β-cell loss induced by treatment with diphtheria toxin or streptozotocin (STZ, a glucose analogue toxic for β-cells) (Fig. 2f–h and Supplementary Table 1d), suggesting that all α-cells can produce insulin. αPdx1OE mice remained hyperglycaemic after β-cell loss, which implies that the insulin-producing α-cells are probably not fully functional (not shown).

We also used DOX to induce another β-cell-specific transcription factor Nkx6.1 in α-cells (Fig. 2i–l). This led to Pdx1 induction, glucagon inhibition and insulin expression in most α-cells, but only after β-cell loss (Fig. 2k,l).

In summary, in intact islets, β-cell transcription factor activity in α-cells is insufficient to trigger insulin protein production. However, results reveal an intrinsic ability of α-cells to produce insulin when combined with β-cell injury. Thus, β-cell loss enhances the capacity of α-cells to produce insulin.

Antagonistic response of α-cells to β-cell loss. To understand how massive β-cell loss influences the α-cell population, we performed RNA-Seq on native α-cells, α-cells one month after diphtheria toxin-induced β-cell ablation (αDT) and native β-cells. We also profiled α-cells expressing Pdx1, that is, α-cells from Pdx1OE mice (αPdx1) that lack glucagon expression and α-cells from Pdx1OE mice one month after diphtheria toxin-induced β-cell loss (αPdx1 + diphtheria toxin) that co-express glucagon and insulin (Fig. 3a and Supplementary Fig. 2). Principal component analyses revealed that αDT, αPdx1 and αPdx1 + diphtheria toxin cells retain a strong α-like gene signature, indicating that they are significantly different from native β-cells (Supplementary Fig. 3a). We filtered all differentially expressed genes between native α- and β-cells (1,682 and 1,258 genes, respectively; false discovery rate (FDR) < 0.01; fold change (FC) > 2; Supplementary Table 2a), assessed how they were impacted in α-cells in all conditions (αDT, αPdx1 and αPdx1 + diphtheria toxin; Supplementary Table 2) and categorized them according to their modulation (up- or downregulated compared to native α-cells; Fig. 3b,c and Supplementary Fig. 3b,c). Fifty-nine α-cell genes were downregulated and 140 β-cell genes were upregulated in the α-cells that did not express insulin after diphtheria toxin administration (Fig. 3b and Supplementary Fig. 3c), which indicates that α-cells acquire some β-cell identity traits following β-cell loss. Concomitantly, 67 α-cell-enriched genes were further upregulated, reinforcing the α-cell signature. This dual response was also observed in α-cells expressing Pdx1 in islets with intact β-cell mass: 238 β-cell genes were induced (*Ins1*, *Ins2*, *Gjd2*, …), 153 α-cell genes were downregulated (*Gcg*, *MafB*, …) and 81 α-cell genes were upregulated. Some of the induced β-cell genes (*Ins1* and *G6pc2)* are direct Pdx1 targets. Thirty-five β-cell-enriched genes were induced by diphtheria toxin or Pdx1 (Fig. 3b).

Although they were not expressed at levels comparable to that of native β-cells, 40% of the β-cell-enriched genes (503 out of 1,258) were upregulated in α-cells expressing Pdx1 when β-cells were ablated (Fig. 3b; αPdx1 + diphtheria toxin). Interestingly, Pdx1 was expressed in these α-cells at levels similar to those observed in β-cells (Fig. 3c). Within these 503 upregulated β-cell genes, 233 (46%) were not significantly induced by diphtheria toxin or Pdx1 alone (Fig. 3d). Similarly, 238 (66%) of the 361 downregulated α-cell genes in αPdx1 + diphtheria toxin cells, were not significantly modulated by Pdx1 activity alone or after β-cell loss (Fig. 3b,c and Supplementary Fig. 3c).

These results indicate that β-cell loss facilitates the expression of β-cell-enriched genes in α-cells. This correlates with the strong induction of insulin in most αPdx1 cells after β-cell ablation (Supplementary Fig. 3). Massive β-cell ablation decreases the α-cell expression of some α-cell-enriched genes; this is accentuated when combined with Pdx1 induction. Also, other α-cell-enriched genes were further upregulated, indicating that these conditions alter α-cell identity in antagonistic ways.

Insulin deprivation leads to α-cell identity changes. Our results suggest that massive β-cell loss is a requisite for spontaneous α-cell conversion. We therefore hypothesized that active insulin signalling in α-cells may prevent these cells from producing insulin. We assessed whether insulin signalling is compromised in α-cells after β-cell depletion on sorted Venus$^+$ α-cells from *glucagon-Venus, RIP-DTR* mice, five days after β-cell ablation induction (Supplementary

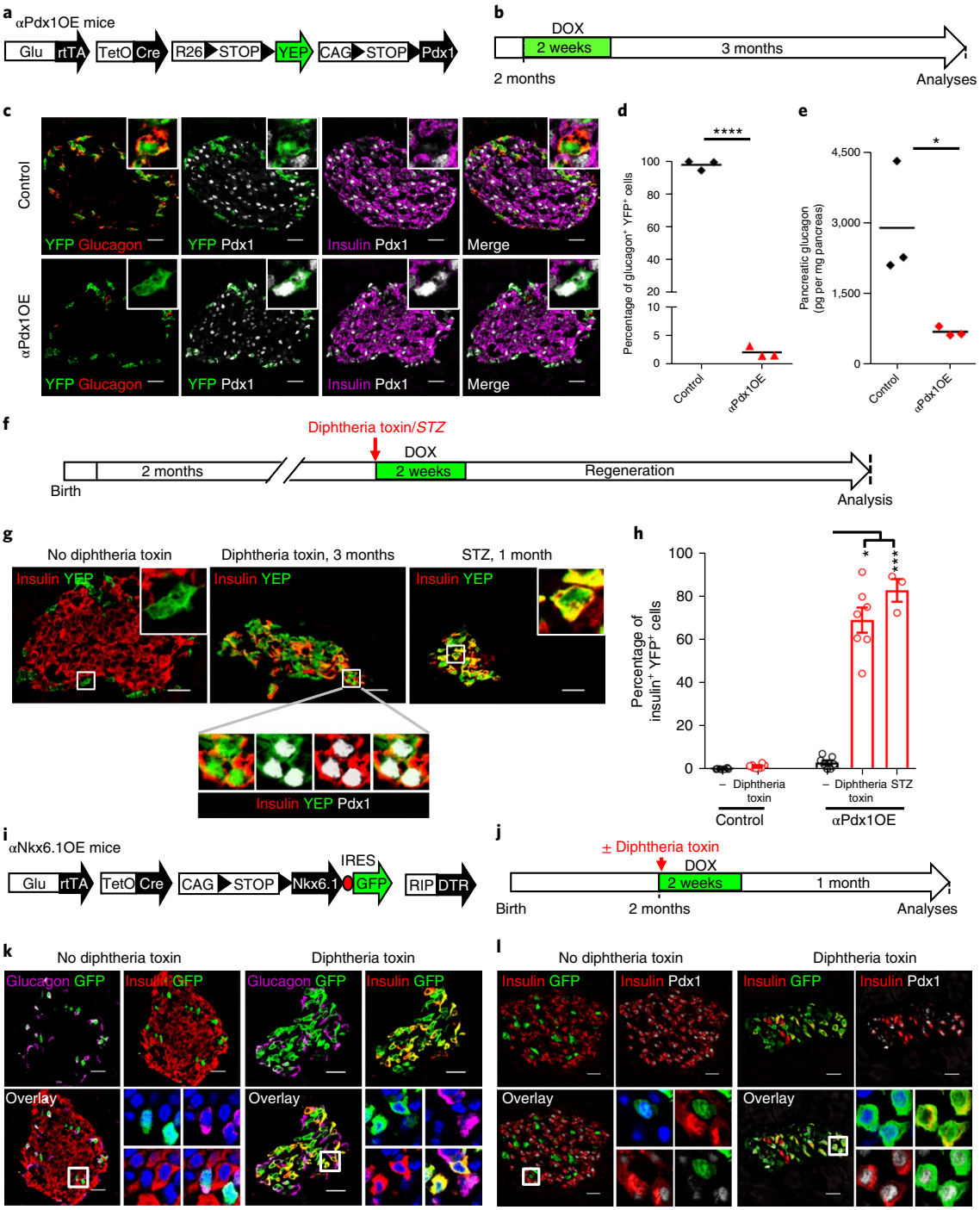

Fig. 2 | Pdx1 expression inhibits glucagon production in adult α-cells. a, Transgenes required for α-cell tracing and ectopic Pdx1 expression. **b**, Experimental design. **c**, α-cells are specifically and efficiently YFP-labelled following DOX administration in controls (upper panel). Pdx1-expressing YFP$^+$ α-cells cease glucagon expression (bottom panel). The experiment was performed once. **d**, Percentage of YFP$^+$ α-cells expressing glucagon after Pdx1 expression. Two-tailed unpaired *t*-test, $P < 0.0001$; $n = 3$ for both control and α-PdxOE mice. **e**, Pancreatic glucagon content is decreased in αPdx1OE mice. Two-tailed unpaired *t*-test, $P = 0.0362$; $n = 3$ for both control and α-PdxOE mice. **f**, Experimental design for Pdx1 induction in α-cells and diphtheria toxin- or STZ-triggered β-cell loss. **g**, A vast fraction of YFP$^+$ α-cells (that express Pdx1) start insulin production after diphtheria toxin- or STZ-mediated β-cell loss. The experiment was performed once with mice treated asynchronously according to their availability. **h**, Percentage of YFP$^+$ α-cells expressing insulin in αPdx1OE mice after β-cell loss. Two-tailed Mann–Whitney test; STZ + Pdx1 versus Pdx1, $P = 0.0167$; diphtheria toxin + Pdx1 versus Pdx1, $P = 0.0006$; $n = 6$ and 8 for untreated and diphtheria toxin-treated control mice, respectively; $n = 7$, 7 and 3 for untreated, diphtheria toxin- and STZ-treated α-PdxOE mice, respectively. **i**, Transgenes required for α-cell tracing, diphtheria toxin-mediated β-cell ablation and ectopic Nkx6.1 expression. **j**, Experimental design. **k**, Nkx6.1 expression (GFP$^+$ cells) does not induce insulin production in α-cells in the presence of a normal β-cell mass. Glucagon expression persists in Nkx6.1OE α-cells (upper lane). After diphtheria toxin-mediated β-cell loss, most Nkx6.1-expressing α-cells start insulin expression and stop glucagon production (bottom lane). The experiment was performed once with all animals treated asynchronously according to their availability. **l**, Pdx1 is not expressed in Nkx6.1OE α-cells when the β-cell mass is normal (upper lane) but is induced after diphtheria toxin treatment (bottom lane). Mean values in all plots are shown by horizontal bars, error bars indicate s.e.m. *$P < 0.5$, ***$P < 0.001$, ****$P < 0.0001$. Scale bars, 20 μm. See Supplementary Table 1b–d for the source data.

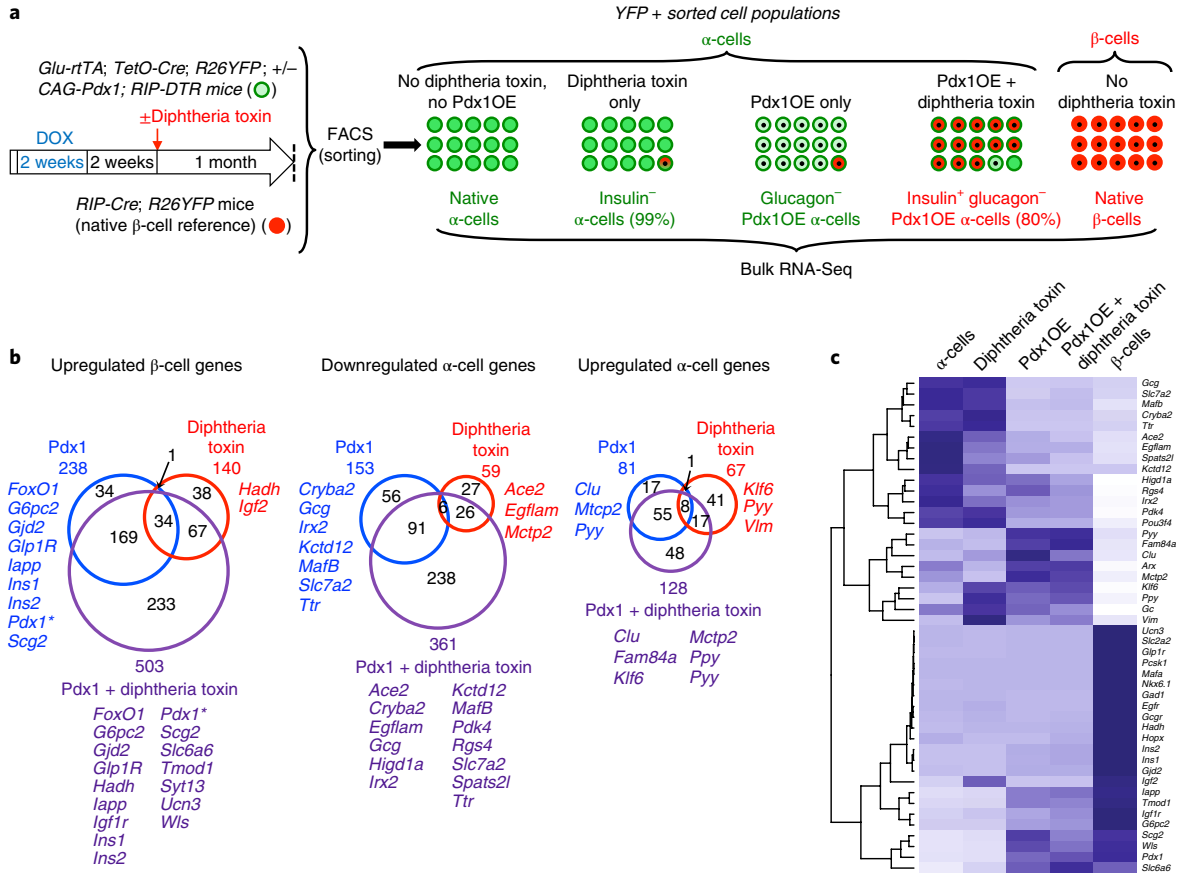

Fig. 3 | Diphtheria toxin-mediated β-cell loss facilitates β-cell gene expression and elicits dual responses in α-cells. a, Experimental design for RNA-Seq. Transgenic mice allowing α- and β-cell lineage tracing were used to sort the following cell populations by fluorescence-activated cell sorting (FACS): native control α-cells ($n=6$ biologically independent samples), α-cells one month after diphtheria toxin-induced β-cell ablation ($n=3$ biologically independent samples), α-cells overexpressing Pdx1 (Pdx1OE, $n=3$ biologically independent samples) and α-cells overexpressing Pdx1 combined with β-cell ablation (Pdx1OE + diphtheria toxin; $n=5$ biologically independent samples). Native β-cells were also collected ($n=5$ biologically independent samples) and analysed to identify differentially expressed genes (DEGs) between native α- and β-cells, as reference gene sets (α- or β-cell genes). Note that insulin protein was detected in only 1% of α-cells in the diphtheria toxin group and 2% in the Pdx1OE group (immunofluorescence). The RNA-Seq experiment was performed once. **b**, Venn diagrams showing the regulation of α- or β-cell-enriched genes in Pdx1OE, diphtheria toxin and Pdx1OE + diphtheria toxin conditions. Differential gene expression was determined for each condition (diphtheria toxin, Pdx1OE and Pdx1OE + diphtheria toxin) compared to native α-cells and intersected with α- or β-cell-enriched genes to identify α- or β-cell signature changes. *Pdx1** indicates that *Pdx1* was identified as differentially expressed but could not be descriminated as either endogenous or transgenic. Numbers refer to the number of genes in each category. The DEGs in the left and middle panels are upregulated β- and downregulated α-cell genes, respectively, which could be considered as an increased β-cell signature in α -cells. Conversely, all genes in the right panel are upregulated α-cell genes, which could represent a resistance to reprogramming. Only representative genes with FDR < 0.05 are shown. The entire gene lists are reported in Table S2. **c**, Heatmap showing scaled expression (blue, high; white, low) of representative α- or β-cell genes in **b** and Supplementary Fig. 3c. The gene clustering shown by the dendrogram indicates separated gene clusters with different modulation patterns in each condition analysed, as seen in **b** and Supplementary Fig. 3. See Supplementary Table 2 for the source data.

Fig. 3d,e). Massive β-cell death triggered a rapid downregulation of insulin-signalling genes in α-cells (Supplementary Fig. 3e). Interestingly, insulin-like growth factor 1 (*Igf1*), an activator of the insulin-signalling pathway, was upregulated in β-cell-depleted islets (Supplementary Fig. 3f), probably as a compensatory attempt to maintain insulin/IGF1 signalling in islets. This confirms that insulin signalling is active in α-cells under physiological conditions and is blunted after β-cell loss. Gene set enrichment analyses from RNA sequencing (RNA-Seq) indicate that insulin receptor signalling pathways (PKC activity and PI3K binding) are modulated in α-cells following β-cell ablation (Supplementary Fig. 3g).

To investigate whether local insulin deprivation alters α-cell identity, we genetically or pharmacologically impaired insulin/IGF1 receptor signalling in healthy mice. Through DOX administration to α-IR/IGF1R-KO mice, insulin and IGF1 receptors (insulin receptor and IGF1R) were downregulated and YFP was activated in α-cells (Fig. 4a,b). This led to *Ins1*, *Nkx6.1* and *Pdx1* transcript upregulation in α-cells, although insulin was not detected at the protein level (Fig. 4c,d). Therefore, the downregulation of insulin/IGF1 signalling, specifically in α-cells, initiates insulin gene transcription. We speculate that a more efficient inactivation of IR/IGF1R genes in α-cells, and perhaps in all non-β islet cell types, would lead to stronger upregulation of β-cell genes. Furthermore, the observed upregulation of IRS2 probably compensates in part the effects of IR/IGF1R downregulation.

In parallel, we transiently blocked insulin action using the insulin receptor antagonist S961 (Novo Nordisk)[17–19], which induces hyperglycaemia and insulin resistance. Healthy *Glucagon-rtTA*; *TetO-Cre*; *R26-YFP* mice were treated with DOX to tag α-cells and then with S961 (Fig. 4e). Mice were either analysed during S961 treatment

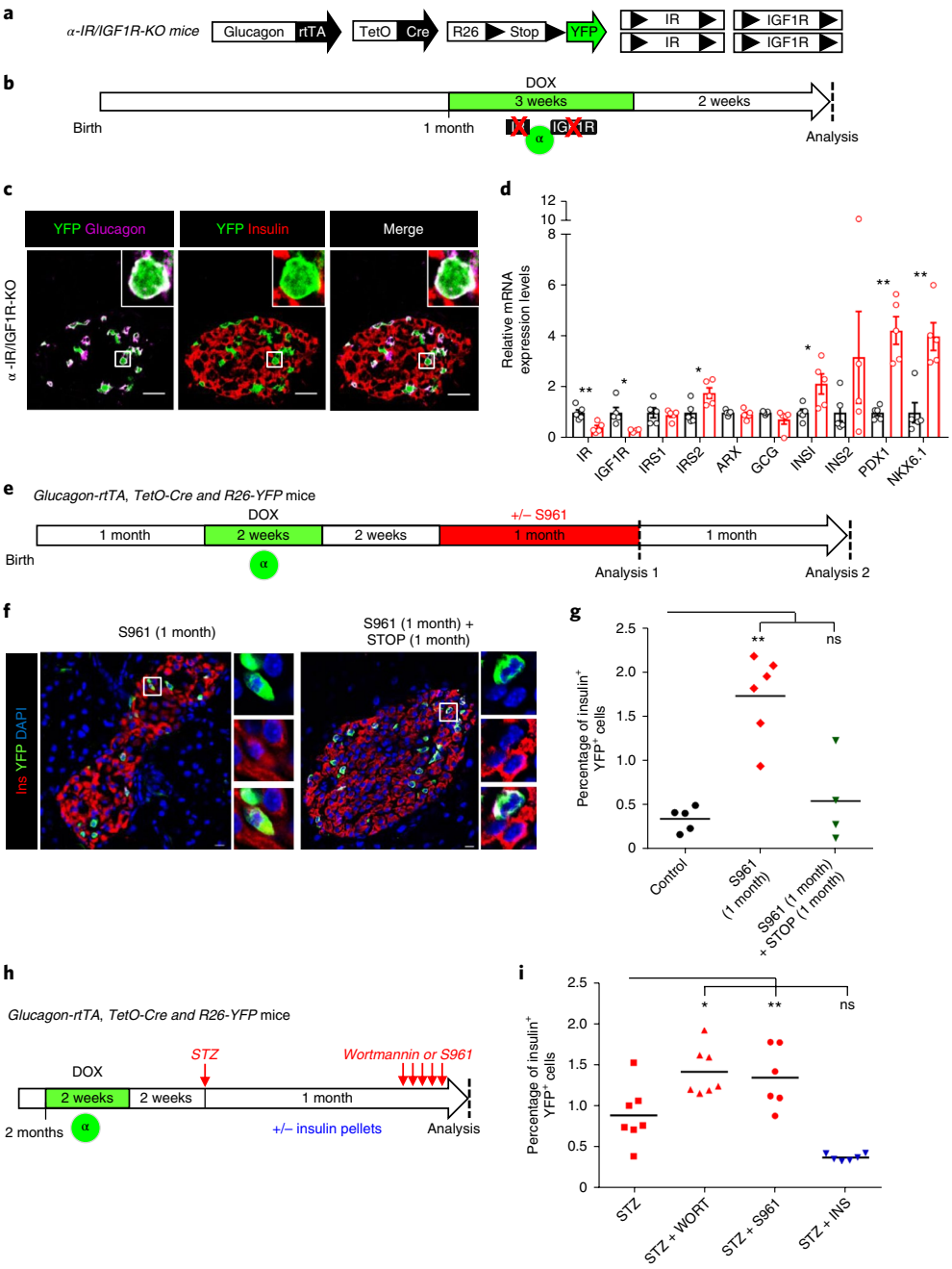

Fig. 4 | Decreased insulin signalling predisposes α-cells to insulin production in islets with an intact β-cell mass. a, Transgenes for α-cell tracing and insulin receptor (IR) and IGF1 receptor (IGF1R) downregulation in adult α-cells. **b**, Experimental design. **c**,**d**, Immunofluorescence on islets (**c**) and RT-qPCR of purified YFP⁺ α-cells from αIR/IGF1R KO mice (**d**). Impaired insulin/IGF1 signalling does not lead to insulin protein production but induces insulin, Pdx1 and Nkx6.1 gene expression. Black bars indicate mice with intact insulin IGF1R signalling (cnt mice); red bars indicate mice in which insulin and IGF1R signalling are compromised. Data are shown as mean ± s.e.m.; $n = 5$ independent biological samples (that is, one mouse or pool of mice per sample); two-tailed Mann–Whitney test (IR, $P = 0.0079$; IGF1R, $P = 0.0159$; IRS2, $P = 0.0317$; INS1, $P = 0.0317$; PDX1, $P = 0.0079$ and NKX6.1, $P = 0.0079$). The experiment was performed once. **e**, Experimental design for α-cell tracing and insulin signalling blockade with S961 in mice with intact β-cell mass. Islets were analysed either immediately after stopping S961 (analysis 1) or one month later (analysis 2). **f**, Immunofluorescence of islets from S961-treated mice. YFP⁺ α-cells expressing insulin are present only in islets of mice analysed during S961 treatment (analysis 1). The experiment was performed once on 3–5 consecutive sections per animal with similar results. The mice were treated asynchronously according to their availability. **g**, Percentage of YFP⁺ α-cells expressing insulin after treatment with or without S961 treatment (analyses 1 and 2). Horizontal bars indicate the mean; $n = 5$, 6 and 4 animals for control (no treatment), S961 (1 month) and S961 (1 month) + STOP (1 month), respectively; two-tailed Mann–Whitney test ($P = 0.0025$) comparing S961 (1 month) versus controls. **h**, Experimental design for α-cell tracing and STZ-induced β-cell ablation followed by either blockade of residual insulin signalling with Wortmannin or S961, or insulin-signalling enhancement through insulin administration (subcutaneous pellets). **i**, Percentage of converted α-cells after β-cell loss and inhibition or enhancement of residual insulin signalling. Horizontal bars indicate the mean; $n = 7$ mice for STZ and STZ + WORT groups and $n = 6$ mice for STZ + S961 and STZ + INS groups; two-tailed Mann–Whitney test ($P = 0.0070$, $P = 0.0350$ and $P = 0.0047$ for comparisons of STZ + WORT, STZ + S961 and STZ + INS with STZ, respectively). $^*P < 0.5$, $^{**}P < 0.01$. Scale bars, 10 μm. See Supplementary Table 1e for the source data.

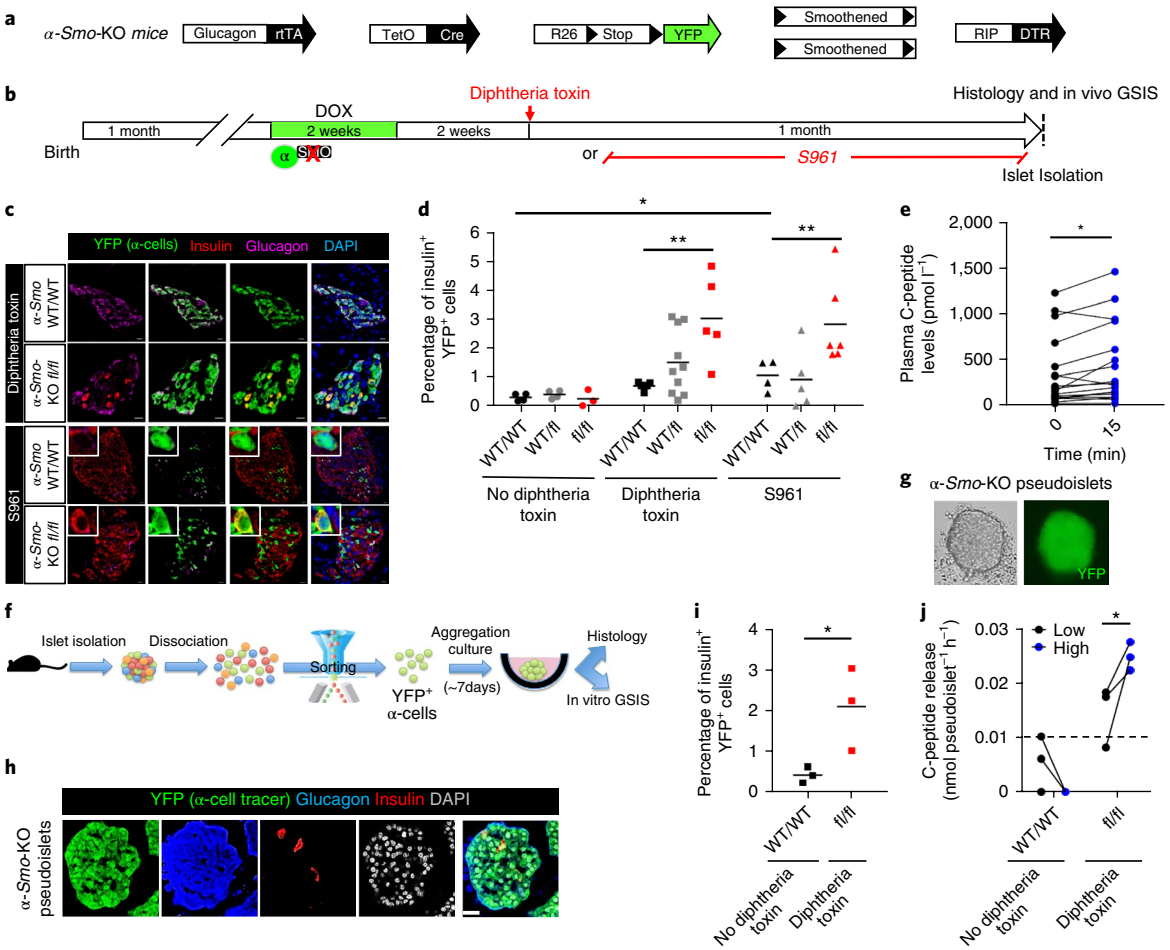

Fig. 5 | *Smo* inactivation in α-cells facilitates their engagement in insulin production. a, Transgenes required for simultaneous α-cell lineage tracing, *Smo* co-receptor downregulation and diphtheria toxin-induced β-cell ablation. **b**, Experimental design. **c**, *Smo* inactivation in α-cells leads to insulin production when combined with β-cell loss (upper panels) or insulin receptor antagonism (lower panels). Immunofluorescence was performed once on 3–5 consecutive sections per animal with similar results. The mice were treated asynchronously according to their availability. Scale bars, 10 µm. GSIS, glucose-stimulated insulin secretion. **d**, Percentage of YFP$^+$ cells producing insulin following the inactivation of *Smo* in α-cells combined with diphtheria toxin or S961 treatment. Treatment groups with no diphtheria toxin, $n=4$, 4 and 3 for Smo$^{WT/WT}$, Smo$^{fl/fl}$ and Smo$^{fl/fl}$ mice, respectively; diphtheria toxin treatment groups, $n=4$, 10 and 5 for Smo$^{WT/WT}$, Smo$^{fl/fl}$ and Smo$^{fl/fl}$ mice, respectively; S961 treatment groups, $n=4$, 5 and 6 for Smo$^{WT/WT}$, Smo$^{fl/fl}$ and Smo$^{fl/fl}$ mice, respectively. Horizontal bars indicate the mean; two-tailed Mann–Whitney test; Smo$^{fl/fl}$ diphtheria toxin versus Smo$^{WT/WT}$ diphtheria toxin treatment, $P=0.0079$; Smo$^{fl/fl}$ diphtheria toxin versus Smo$^{WT/WT}$ S961 treatment, $P=0.0095$; Smo$^{fl/fl}$ S961 versus Smo$^{WT/WT}$ S961 treatment, $P=0.0286$. **e**, In vivo glucose challenge in α-*Smo*-KO mice. Two-tailed Wilcoxon test, $P=0.012$; $n=18$ mice. **f**, Pipeline for α-cell sorting, in vitro pseudoislet reconstruction and functional tests. **g**, Live imaging of seven-day-cultured pseudoislet reconstituted using α-cells from α-*Smo*-KO mice. Representative images from three independent experiments are shown. **h**, Immunofluorescence of α-*Smo*-KO pseudoislet at day seven of aggregation culture. Representative images from three independent experiments are shown. Scale bar, 25 µm. **i**, Percentage of YFP$^+$ cells producing insulin in pseudoislets from control α-*Smo*-WT (no β-cell ablation) or α-*Smo*-KO mice after cell ablation (diphtheria toxin treatment). Three independent cohorts each from 18 α-*Smo*-WT and 18 α-*Smo*-KO mice. Horizontal bars indicate the mean; $P=0.049$, two-tailed unpaired *t*-test. **j**, Glucose-stimulated C-peptide secretion. α-*Smo*-KO cells secrete C-peptide in response to glucose in vitro, whereas α-*Smo*-WT (no diphtheria toxin control) cells have no measurable secretion. Three independent cohorts each from 18 α-*Smo*-Wt and 18 α-*Smo*-KO mice. $P=0.048$, one-tailed paired *t*-test. The dashed line indicates the detection threshold documented by the manufacturer (0.0127 nmol pseudoislet^{-1} h^{-1}). Each data point represents one independent experiment using biologically different samples. $^*P<0.5$, $^{**}P<0.01$. See Supplementary Table 1f–l for the source data.

(analysis 1) or after treatment was stopped (analysis 2). When insulin action was inhibited[13,20], about 2% of the YFP$^+$-traced α-cells expressed insulin (Fig. 4f,g, analysis 1 and Supplementary Table 1e), Pdx1 and Nkx6.1 (Supplementary Fig. 4a–c). Insulin (*Ins1* and *Ins2*) transcripts were upregulated in α-cells sorted from S961-treated *glucagon-Venus* mice (Supplementary Fig. 4d,e). In contrast, when islets were analysed one month after S961 treatment was stopped (Fig. 4e, analysis 2; Supplementary Table 1e), insulin protein became undetectable in α-cells, which suggests that its production had ceased (Fig. 4f,g).

We next combined STZ-induced partial β-cell loss with the pharmacological inhibition of insulin[20,21]. One month after STZ treatment, *Glucagon-rtTA*; *TetO-Cre*; *R26-YFP* mice received either Wortmannin (a PI3K inhibitor) or S961, to inhibit the residual insulin signalling (Fig. 4h). The proportion of α-cells that produce insulin increased following drug treatment compared to mice treated with only STZ (Fig. 4i and Supplementary Table 1e). Conversely, α-cell reprogramming was abrogated when STZ treatment was followed by insulin therapy (Fig. 4i

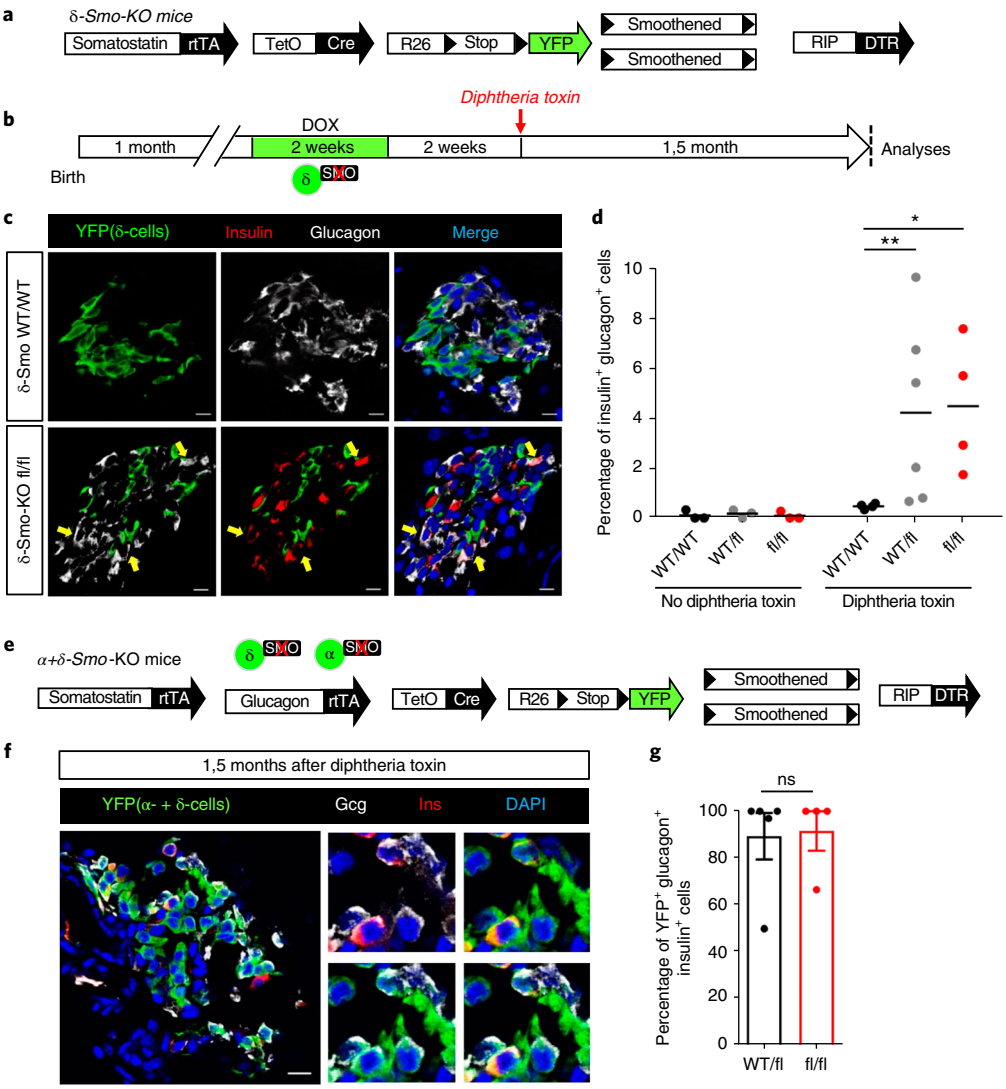

Fig. 6 | *Smo* inactivation in δ-cells leads to enhanced conversion of α-cells β-cells. a, Transgenes required for simultaneous δ-cell lineage tracing, *Smo* co-receptor downregulation and diphtheria toxin-induced β-cell ablation. **b**, Experimental design. **c**, Immunofluorescence staining of islets from δ-*Smo*-KO mice 1,5 months after diphtheria toxin-induced β-cell loss. Mice (δ-*Smo*-KO) display increased numbers of insulin$^+$ and glucagon$^+$ co-expressing cells compared to controls. **d**, Percentage of cells co-expressing insulin and glucagon in δ-*Smo*-KO mice. Treatment groups with no diphtheria toxin, $n=3$ mice for all; diphtheria toxin treatment groups, $n=4$, 6 and 4 for WT/WT, WT/fl and fl/fl mice, respectively. Two-tailed Mann–Whitney test; WT/fl versus WT/WT, $P=0.0095$; fl/fl versus WT/WT, $P=0.0286$. Horizontal bars indicate the mean. **e**, Transgenes for the simultaneous inactivation of *Smo* in α- and δ -cells, along with their lineage tracing, and for diphtheria toxin-induced β-cell ablation. **f**, Immunofluorescence staining of islets from α+δ-*Smo*-KO mice 1,5 months after diphtheria toxin treatment. **g**, Percentage of insulin$^+$ and glucagon$^+$ co-expressing cells traced with YFP. Mean ± s.e.m; two-tailed Mann–Whitney test, $P=0.84$; $n=5$ WT/fl mice, $n=4$ fl/fl mice. $^*P<0.5$, $^{**}P<0.01$, ns, not significant. Experiments in **c**–**f** were repeated two independent times with similar results. Scale bars, 10 μm. See Supplementary Table 1n–p for the source data.

and Supplementary Table 1e), confirming that insulin negatively modulates α-cell plasticity.

When combined with Pdx1 overexpression in αPdx1OE mice, the number of insulin-producing α-cells were greatly increased in all of the conditions described above (Supplementary Fig. 4f–k and Supplementary Table 1d). Importantly, the number of insulin-negative YFP$^+$ α-cells increased again after S961 treatment was stopped (Supplementary Fig. 4j), which indicates that α-cells are maintained after discontinuing insulin production.

These observations suggest that β-cell death per se is not required for insulin gene expression in α-cells. Insulin-signalling deprivation promotes insulin production in α-cells in a reversible manner. Therefore, in homeostatic conditions, islet insulin signalling helps maintaining α-cell identity.

Constitutive Smo-mediated signalling restricts α-cell plasticity. Given that the vast majority of α-cells are apparently unaffected after β-cells loss, we hypothesized that signalling pathways less affected by β-cell injury could convey molecular cues restricting α-cell plasticity, even when insulin signalling is compromised.

Two observations suggest that Smoothened-mediated Hedgehog (SmoHh) signalling could act as an α-cell identity keeper. First, SmoHh components are expressed in α-, β- and δ-cells, and active signalling was reported in intact islets (Supplementary Fig. 5a–c; refs [22,23]). Second, SmoHh is linked to cell differentiation and

maintenance in many organs, including the pancreas[23–26], where it regulates *Pdx1* and *Ins* expression[27,28].

To test whether SmoHh controls α-cell plasticity, we generated *Glucagon-rtTA; TetO-Cre; R26-YFP*; *Smoothened*$^{fl/fl}$ (loxP-flanked); *RIP-DTR* mice (α-*Smo*-KO) (Fig. 5a). One-month-old α-*Smo*-KO mice were DOX-treated to downregulate Smo in α-cells and tag them with YFP (Supplementary Fig. 5e,f). The downregulation of α-cell-*Smo* triggered the downregulation of *Gcg* and *Arx* (two α-cell-specific markers; Supplementary Fig. 5g), suggesting that active SmoHh in α-cells maintains α-cell identity.

Downregulation of α-cell-*Smo* did not trigger insulin production (Supplementary Fig. 5h). Conversely, Smo inactivation along with β-cells loss or S961 treatment (Fig. 5b) increased the percentage of insulin-expressing α-cells (Fig. 5c,d; Supplementary Table 1f). Hence, downregulation of SmoHh facilitates α-cell reprogramming when combined with insulin-signalling inhibition.

We next examined whether insulin-producing α-cells secrete insulin in response to glucose. As these cells are rare, we took advantage of their increased number in the islets of diphtheria toxin-treated α-*Smo*-KO mice. C-peptide was released in a glucose-responsive manner in the blood of α-*Smo*-KO mice, one month after β-cell ablation (Fig. 5e and Supplementary Table 1g). To determine the precise contribution of converted α-cells and of escaping β-cells (<0.5%), we assessed insulin secretion from α-cells in vitro. We isolated islets from α-*Smo*-KO$^{fl/fl}$ and α-*Smo*-KO$^{WT/WT}$ mice after β-cell loss (Supplementary Table 1h), sorted YFP$^+$ α-cells and re-aggregated them to reconstitute highly purified 'monotypic pseudoislets' (Fig. 5f,g). We confirmed the increased insulin production in these α-cells by immunofluorescence (Fig. 5h,i and Supplementary Table 1i) and performed glucose-stimulated insulin secretion tests in vitro. Pseudoislets from α-*Smo*-KO mice secreted C-peptide in a glucose-dependent manner (Fig. 5j and Supplementary Table 1l). These results suggest that insulin-producing α-cells are functional and naturally secrete insulin in response to glucose.

δ-cells restrict α-cell plasticity. A percentage of δ-cells produce insulin following β-cell loss[12]. As we observed that SmoHh-mediated signalling is active in δ-cells (Supplementary Fig. 5a–c), we investigated its putative role in blocking δ-cell plasticity by downregulating it in *Somatostatin-rtTA*; *TetO-Cre; R26-YFP; Smoothened*$^{fl/fl}$; *RIP-DTR* mice (δ-Smo-KO) (Fig. 6a and Supplementary Fig. 5i,j).

In δ-Smo-KO mice, DOX induces δ-cells Smo downregulation along with YFP-labelling (Supplementary Fig. 5i,j and Supplementary Table 1m).

Downregulation of *Smo* did not affect δ-cell-specific gene expression or induced insulin production (Supplementary Fig. 5j and Supplementary Table 1n). After β-cell ablation, the percentage of δ-cells engaging insulin expression was similar in the control and δ-Smo-KO mice (Supplementary Fig. 5k and Supplementary Table 1n). Yet, surprisingly, the number of glucagon$^+$insulin$^+$ bihormonal cells was ten-fold higher in mice with *Smo* downregulated in δ-cells compared to WT mice (Fig. 6b–d; Supplementary Table 1o). These bihormonal cells were not YFP$^+$-traced, indicating that they were not reprogrammed δ-cells (Fig. 6c). This suggests a potent δ-cell-mediated non-α-cell-autonomous regulation of α-cell plasticity.

To further explore this non-cell-autonomous regulation of α-cell identity, we generated α+δ-Smo-KO mice (*Glucagon-rtTA*; *Somatostatin-rtTA*; *TetO-Cre*; *R26-YFP*; *Smoothened*$^{fl/fl}$; *RIP-DTR*), to inactivate Smo in α- and δ-cells (Fig. 6e). In this situation, the glucagon$^+$ and insulin$^+$ bihormonal cells were YFP$^+$-traced (Fig. 6f,g and Supplementary Table 1p), thus suggesting their α-cell origin.

Pharmacological inhibition of SmoHh with the Hh-signalling inhibitor GANT61 also increased the number of insulin-producing α-cells after β-cell loss (Supplementary Fig. 5l,m).

These observations suggest that active SmoHh-mediated signalling in δ-cells is a non-cell-autonomous intra-islet inhibitory signal that restricts α-cell plasticity in β-cell-ablated islets.

Co-ablation of δ- and β-cells enhances α-cell conversion. To further confirm that δ-cells act as negative regulators of α-cell plasticity, we generated *Somatostatin-Cre*; *R26-YFP*; *R26-iDTR*; *RIP-DTR* mice, to co-ablate β- and δ-cells simultaneously (Supplementary Fig. 5n). The loss of β- and δ-cells doubled the proportion of glucagon$^+$ and insulin$^+$ bihormonal cells (Supplementary Fig. 5n and Supplementary Table 1q). This result is compatible with a δ-cell-mediated restriction of α-cell plasticity.

Discussion

Maintenance of adult cell identity is a highly dynamic process that depends on the tight convergence of diverse signals whose complexity might be correlated with the regenerative capacity of tissues. The pressure to preserve cell identity is probably stronger in highly specialized cells implicated in vital metabolic processes. Endodermal cells may be intrinsically different, always in a 'regenerative state', because they are exposed to external insults[1]. Any uncontrolled phenotypic instability could be detrimental and result in the onset of disease.

Our results show that the near-total loss of β-cells triggers simultaneous signals with antagonistic effects on α-cells: they activate insulin production and favour regeneration while also increasing α-cell marker expression, seemingly enforcing the α-cell fate and opposing identity changes.

We have identified paracrine repressive signals that maintain α-cell identity. We show here that α-cell identity is tightly maintained under physiological conditions through the constant repressive influence of local insulin and SmoHh signalling, originating from proximate β- and δ-cells; the inhibition of proximate β- and δ-cells leads to a substantial increase in insulin$^+$ α-cell numbers. Thus, in addition to regulating α-cell function through somatostatin and insulin, δ- and β-cells ensure α-cell fate maintenance in a non-α-cell-autonomous manner. Even with dual Smo-Ins downregulation, α-cell conversion is only partially improved, which suggests that α-cell conversion is restricted by the synergistic influence of multiple signals. Recent studies on transcription factors expressed in β-cells (such as Pdx1, Nkx6.1, Nkx2.2 and Pax6) suggest that they are directly involved in repressing non-β-cell genes[29–35]. The extracellular repressive signals that lock α-cells in their state may therefore be transmitted via such transcriptional repressors.

The maintenance of cell identity detected in the critical, physiologically relevant islets may be much more widespread in differentiated cells, similar to a natural 'tendency' or 'capacity' of adult mature cells, and appears to be subtler than the complete iPSC reprogramming, with several levels of control of switching of cell phenotype.

This has remarkable implications for our comprehension of how the cell identity–differentiation equilibrium is established.

Our results indicate that spontaneous insulin production in α -cells is not simply due to uncontrolled stress-induced insulin gene dysregulation, but is dynamically regulated, representing a meaningful compensatory response to cope with situations of insulin insufficiency.

Importantly, Lee et al. reported the appearance of insulin-resistant α-cells during diabetes[36]. We propose that these insulin-resistant α-cells would be more susceptible to changes in their identity, allowing them to better cope with insulin deficiency. In agreement with such a speculation, bihormonal cells have been reported in the pancreas of diabetic patients[37,38]. The similarity of insulin-producing α-cells to native β-cells and their level of maturity were not addressed in this study and should be investigated.

In the context of this study, α-cell recruitment into insulin production, encompassing the reduction of glucagon expression, would

also be beneficial for diabetics by limiting glucagon secretion and hepatic glucose mobilization, without major metabolic defects caused by α-cell deficit[39,40].

In conclusion, we have found that the stability of cell identity is heavily context-dependent and not 'carved in stone', with several levels of control on the switching of cell phenotype. A physiological input from signalling pathways inside the islet keeps the identity of the cells in homeostasis. The endocrine-cell plasticity detected in this critical organ may be much more widespread in differentiated cells, akin to the natural tendencies of adult mature cells. Maintaining cell identity is therefore an active process of repressive signals released from surrounding neighbour cells, blocking an intrinsic tendency of specialized differentiated cells to modify their phenotype and functional characteristics (Supplementary Fig. 6).

Online content

Any methods, additional references, Nature Research reporting summaries, source data, statements of data availability and associated accession codes are available at https://doi.org/10.1038/s41556-018-0216-y.

Received: 5 December 2017; Accepted: 17 September 2018;
Published online: 22 October 2018

References

1. Holmberg, J. & Perlmann, T. Maintaining differentiated cellular identity. *Nat. Rev. Genet.* **13**, 429–439 (2012).
2. Thowfeequ, S., Myatt, E. J. & Tosh, D. Transdifferentiation in developmental biology, disease, and in therapy. *Dev. Dynam.* **236**, 3208–3217 (2007).
3. Chera, S. & Herrera, P. L. Regeneration of pancreatic insulin-producing cells by in situ adaptive cell conversion. *Curr. Opin. Genet. Dev.* **40**, 1–10 (2016).
4. Pasque, V., Jullien, J., Miyamoto, K., Halley-Stott, R. P. & Gurdon, J. B. Epigenetic factors influencing resistance to nuclear reprogramming. *Trends Genet.* **27**, 516–525 (2011).
5. Natoli, G. Maintaining cell identity through global control of genomic organization. *Immunity* **33**, 12–24 (2010).
6. Barrero, M. J., Boue, S. & Izpisua Belmonte, J. C. Epigenetic mechanisms that regulate cell identity. *Cell Stem Cell* **7**, 565–570 (2010).
7. Szabat, M. et al. Maintenance of beta-cell maturity and plasticity in the adult pancreas: developmental biology concepts in adult physiology. *Diabetes* **61**, 1365–1371 (2012).
8. Eade, K. T. & Allan, D. W. Neuronal phenotype in the mature nervous system is maintained by persistent retrograde bone morphogenetic protein signaling. *J. Neurosci.* **29**, 3852–3864 (2009).
9. Lopez-Coviella, I., Berse, B., Krauss, R., Thies, R. S. & Blusztajn, J. K. Induction and maintenance of the neuronal cholinergic phenotype in the central nervous system by BMP-9. *Science* **289**, 313–316 (2000).
10. Jessen, K. R., Mirsky, R. & Arthur-Farraj, P. The role of cell plasticity in tissue repair: adaptive cellular reprogramming. *Dev. Cell* **34**, 613–620 (2015).
11. Knapp, D. & Tanaka, E. M. Regeneration and reprogramming. *Curr. Opin. Genet. Dev.* **22**, 485–493 (2012).
12. Chera, S. et al. Diabetes recovery by age-dependent conversion of pancreatic delta-cells into insulin producers. *Nature* **514**, 503–507 (2014).
13. Thorel, F. et al. Conversion of adult pancreatic alpha-cells to beta-cells after extreme beta-cell loss. *Nature* **464**, 1149–1154 (2010).
14. Chakravarthy, H. et al. Converting adult pancreatic islet alpha cells into beta Cells by targeting both *Dnmt1* and *Arx*. *Cell. Metab.* **25**, 622–634 (2017).
15. Bosma, M. J. & Carroll, A. M. The SCID mouse mutant: definition, characterization, and potential uses. *Annu. Rev. Immunol.* **9**, 323–350 (1991).
16. Yang, Y. P., Thorel, F., Boyer, D. F., Herrera, P. L. & Wright, C. V. Context-specific alpha- to-beta-cell reprogramming by forced Pdx1 expression. *Genes Dev.* **25**, 1680–1685 (2011).
17. Schaffer, L. et al. A novel high-affinity peptide antagonist to the insulin receptor. *Biochem. Biophys. Res. Commun.* **376**, 380–383 (2008).
18. Vikram, A. & Jena, G. S961, an insulin receptor antagonist causes hyperinsulinemia, insulin-resistance and depletion of energy stores in rats. *Biochem. Biophys. Res. Commun.* **398**, 260–265 (2010).
19. Yi, P., Park, J. S. & Melton, D. A. Betatrophin: a hormone that controls pancreatic beta cell proliferation. *Cell* **153**, 747–758 (2013).
20. Cigliola, V., Thorel, F., Chera, S. & Herrera, P. L. Stress-induced adaptive islet cell identity changes. *Diabetes Obes. Metab.* **18**, 87–96 (2016).
21. Damond, N. et al. Blockade of glucagon signaling prevents or reverses diabetes onset only if residual beta-cells persist. *eLife* **5**, e13828 (2016).
22. Grieco, F. A. et al. Delta-cell-specific expression of hedgehog pathway Ptch1 receptor in murine and human endocrine pancreas. *Diabetes Metab. Res. Rev.* **27**, 755–760 (2011).
23. Lau, J. & Hebrok, M. Hedgehog signaling in pancreas epithelium regulates embryonic organ formation and adult beta-cell function. *Diabetes* **59**, 1211–1221 (2010).
24. Kawahira, H. et al. Combined activities of hedgehog signaling inhibitors regulate pancreas development. *Development* **130**, 4871–4879 (2003).
25. Cervantes, S., Lau, J., Cano, D. A., Borromeo-Austin, C. & Hebrok, M. Primary cilia regulate Gli/Hedgehog activation in pancreas. *Proc. Natl Acad. Sci. USA* **107**, 10109–10114 (2010).
26. Landsman, L., Parent, A. & Hebrok, M. Elevated Hedgehog/Gli signaling causes beta-cell dedifferentiation in mice. *Proc. Natl Acad. Sci. USA* **108**, 17010–17015 (2011).
27. Thomas, M. K., Lee, J. H., Rastalsky, N. & Habener, J. F. Hedgehog signaling regulation of homeodomain protein islet duodenum homeobox-1 expression in pancreatic beta-cells. *Endocrinology* **142**, 1033–1040 (2001).
28. Thomas, M. K., Rastalsky, N., Lee, J. H. & Habener, J. F. Hedgehog signaling regulation of insulin production by pancreatic beta-cells. *Diabetes* **49**, 2039–2047 (2000).
29. Schaffer, A. E. et al. Nkx6.1 controls a gene regulatory network required for establishing and maintaining pancreatic Beta cell identity. *PLoS Genet.* **9**, e1003274 (2013).
30. Gao, T. et al. Pdx1 maintains beta cell identity and function by repressing an alpha cell program. *Cell Metab.* **19**, 259–271 (2014).
31. Gutierrez, G. D. et al. Pancreatic beta cell identity requires continual repression of non-beta cell programs. *J. Clin. Invest.* **127**, 244–259 (2017).
32. Swisa, A. et al. PAX6 maintains beta cell identity by repressing genes of alternative islet cell types. *J. Clin. Invest.* **127**, 230–243 (2017).
33. Papizan, J. B. et al. Nkx2.2 repressor complex regulates islet beta-cell specification and prevents beta-to-alpha-cell reprogramming. *Genes Dev.* **25**, 2291–2305 (2011).
34. Gauthier, B. R., Gosmain, Y., Mamin, A. & Philippe, J. The beta-cell specific transcription factor Nkx6.1 inhibits glucagon gene transcription by interfering with Pax6. *Biochem. J.* **403**, 593–601 (2007).
35. Schisler, J. C. et al. The Nkx6.1 homeodomain transcription factor suppresses glucagon expression and regulates glucose-stimulated insulin secretion in islet beta cells. *Proc. Natl Acad. Sci. USA* **102**, 7297–7302 (2005).
36. Lee, Y. et al. Hyperglycemia in rodent models of type 2 diabetes requires insulin-resistant alpha cells. *Proc. Natl Acad. Sci. USA* **111**, 13217–13222 (2014).
37. Butler, A. E. et al. Adaptive changes in pancreatic beta cell fractional area and beta cell turnover in human pregnancy. *Diabetologia* **53**, 2167–2176 (2010).
38. White, M. G. et al. Expression of mesenchymal and alpha-cell phenotypic markers in islet beta-cells in recently diagnosed diabetes. *Diabetes Care* **36**, 3818–3820 (2013).
39. Thorel, F. et al. Normal glucagon signaling and beta-cell function after near-total alpha-cell ablation in adult mice. *Diabetes* **60**, 2872–2882 (2011).
40. Hayashi, Y. et al. Mice deficient for glucagon gene-derived peptides display normoglycemia and hyperplasia of islet α-cells but not of intestinal L-cells. *Mol. Endocrinol.* **23**, 1990–1999 (2009).

Acknowledgements

We are grateful to Y. Dor, A. Ruiz i Altaba and M. González Gaitán for carefully reading and discussing the manuscript; to O. Fazio, M. Urwyler, C. Gysler, B. Polat and R. Gangula for their technical help and to J.-P. Aubry-Lachainaye for FACS assistance. We acknowledge C. Delucinge-Vivier, M. Docquier, A. Efanov, P. Ebert, J. Calley, H. Wu, S.K. Syed and T. Wei for technical and expert assistance supporting RNA sequencing, quality control, statistical and bioinformatics analyses. M.S. was supported by R01DK068471 (NIH/NIDDK). S.C. is supported by grants from the Research Council of Norway (NFR no. 247577) and the Novo Nordisk Foundation (no. NNF15OC0015054). M.A.M. was supported by U01DK072473 (Beta Cell Biology Consortium). Work was funded by grants from the National Institutes of Health/National Institute of Diabetes and Digestive and Kidney Disease (Beta Cell Biology Consortium, grant no. U01DK089566 and Human Islet Research Network, grant nos UC4-DK104209 and UC4-DK108132), the Juvenile Diabetes Research Foundation (in part through joint research funding with Lilly Research Laboratories, grant nos 17-2011-276, and 2-SRA-2015-67-Q-R), the Innovative Medicines Initiative Joint Undertaking under grant agreement no. 155005 (IMIDIA), resources of which are composed of financial contribution from the European Union's Seventh Framework Programme (FP7/2007-2013) and EFPIA companies' in kind contribution, the Fondation privée des Hôpitaux Universitaires de Genève–Confirm, the Fondation Aclon and the Swiss National Science Foundation (grant no. NRP63, 310030_152965 and the Bonus of Excellence grant no.310030B_173319) to P.L.H.

Author contributions

V.C., F.T., L.G., S.C., D.B. and K.F. performed all of the experiments and most analyses. T.M., H.K, C.E.V.W. and M.S. provided transgenic lines. M.K.T., S.G., S.C., K.F. and L.V.G analysed RNA-Seq data. M.A.M. and A.B.O. generated the *Sst-rtTA* knock-in mouse line. K.F., F.T., V.C., L.G., S.C., D.O. and P.L.H. conceived the experiments and wrote the manuscript.

Competing interests

The authors declare no competing interests.

Additional information

Supplementary information is available for this paper at https://doi.org/10.1038/s41556-018-0216-y.

Reprints and permissions information is available at www.nature.com/reprints.

Correspondence and requests for materials should be addressed to P.L.H.

Publisher's note: Springer Nature remains neutral with regard to jurisdictional claims in published maps and institutional affiliations.

Methods

Mice. Transgenic mice were described in earlier work[12,13,16,41–44]. *Sst*^{rtTA} knock-in mice were genetically engineered as follows: a *Sst*$^{rtTA.LCA}$ allele was made using a targeting vector made by BAC recombineering starting with BAC clone RP23-274H19 (purchased from CHORI). Both the general strategy and vectors were previously described[45]. The targeting vector, pSst.rtTA.LCA, contained a 5′ homology arm of 7.3 kb and a 3′ homology arm of 3.6 kb flanking a *Lox66* site, a modified region of the Sst gene containing the reverse tetracycline TransActivator (rtTA) and a Lox2272 site. The cassette contained both a PGK-puromycinΔ thymidine kinase and EM7-kanamycin selectable markers flanked by two tandemly-oriented FRT sites. After electroporation of the targeting vector into 129S6-derived mouse ES cells, 192 puromycin-resistant clones were obtained, 24 of which had undergone the desired homologous recombination event. Clone 1A8 was used to derive chimeras that were then bred with C57BL/6J mice to obtain germline transmission. The FRT-flanked selectable markers were removed by interbreeding with a FlpE-expressing transgenic mouse[46].

Male and female mice were used for all experiments, except for transplantation experiments, for which only males were used as hosts. The animals were treated with care and respect. This study is compliant with all relevant ethical regulations regarding animal research and all experiments have been approved and performed according to the guidelines of the Direction générale de la santé du Canton de Genève (license numbers: GE/103/14; GE/111/17 and GE/121/17). The number of mice used was limited by the availability of the required complex genotype. The mice were randomly selected for treatments and control. The sample sizes were in the range of the published literature and exclusion criteria were transgene set, general health status and occasional spontaneous death during the experiments.

Diphtheria toxin, DOX, STZ, S961, wortmannin and insulin treatments. Diphtheria toxin (Sigma) was administrated by intra-peritoneal injections as previously described[13]. DOX (1 mg ml^{-1}; Sigma) was added to the drinking water. STZ was injected intraperitoneally as a single dose (200 mg per kg body weight). S961 (Novo Nordisk) was given via ALZET osmotic pumps implanted subcutaneously (40 nmol per week). Wortmannin (Sigma) was intraperitoneally injected daily for five consecutive days (1 mg per kg body weight). Mice received a subcutaneous insulin pellet (Linbit) when glycaemia exceeded 25 mM.

Islet isolation, FACS, RNA extraction and qPCR. Islet isolation, cell sorting, RNA preparation and qPCR were performed as described in earlier work[12]. All qPCRs were performed in triplicate. Primers are listed in Supplementary Table 3. Components of the insulin signalling pathway were evaluated with the *PAMM-030Z* and qPCR were performed as previously reported[12].

Non-quantitative RT-PCR. Total RNA was isolated from the liver, uterus and duodenum and used as controls. Tissue RNA was prepared using the Qiagen RNeasy Mini Kit. Islets cells were FAC-sorted as previously described[12] and RNA prepared using the Qiagen RNeasy Micro Kit. The Qiagen QuantiTect Reverse Transcription Kit was used to prepare cDNA starting from 1 µg of RNA. Amplification conditions and primers were as previously reported[47,48]. Primers for actin were unpublished and are reported in Supplementary Table 3.

RNA sequencing and quality control. Islet isolation and cell isolation by FACS were performed using previously published protocols[12]. The gating strategy used for FACS sorting is provided in Supplementary Fig. 2. The experimental design for sample collection is reported in Fig. 2a. Briefly, purified cells were obtained as follows: (1) native α-cells from three-month-old *Glucagon-rtTA*; *TetO-Cre*; *Rosa26YFP*; *RIP-DTR* mice, (2) αDT: α-cells from *Glucagon-rtTA*; *TetO-Cre*; *Rosa26YFP*; *RIP-DTR* mice one month after diphtheria toxin treatment, (3) αPdx1OE: α-cells ectopically expressing PDX1 from three-month-old *Glucagon-rtTA*; *TetO-Cre*; *R26YFP*; *CAG-Pdx1*; *RIP-DTR* mice, (4) αPdx1OE + DT: α-cells expressing PDX1 from *Glucagon-rtTA*; *TetO-Cre*; *R26YFP*; *CAG-Pdx1*; *RIP-DTR* mice one month after diphtheria toxin treatment and (5) native β-cells from 3-month-old *RIP-Cre* and *Rosa26YFP* mice.

Extracted RNA was assessed for quality by an Agilent bioanalyzer. Libraries were prepared (according to Illumina's standard protocols), multiplexed and sequenced on an Illumina platform with paired-end 100-bp reads. The sequencing quality control was done with FASTQC v.0.10.1, followed by sequence alignment to the mouse reference genome (UCSC mm10) using the TopHat v2.0.9 (default parameters). Biological quality control and summarization were done with the RSeQC v2.4, the PicardTools v1.92 and the SamTools v0.1.18. In brief, RNA sequencing quality for each sample was assessed for overall coverage, base composition, presence of adaptors and 3′ bias, among other factors. A subset of samples were excluded from further analyses due to poor sequencing quality, 3′ bias, contamination or outlier status for technical or biological reasons, including outliers on the first principal component analysis across the entire sample set or samples with PDX-1 expression levels exceeding 3 s.d. from the mean of each respective experimental group. Finally, 22 samples were included for all downstream analyses ($n = 6$ for native α-cells, $n = 3$ for αDT, $n = 3$ for αPdx1OE, $n = 5$ for αPdx1OE + diphtheria toxin and $n = 5$ for native β-cells). The raw count data was prepared with HTSeq v.0.6.1p1 (htseq-count, defaults parameters). The RNA-Seq data generated in this study have been deposited in the NCBI GEO database under accession number GSE109285.

Transcriptomic data analyses. The normalization and differential expression analysis was performed with the R/Bioconductor package edgeR package v.3.20.9. Briefly, genes expressed at very low levels were filtered out and genes that achieved ten counts in at least five samples were kept. The filtered data were normalized by the library size and DEGs were estimated with the negative binomial general model statistics. To identify DEGs, pairwise comparisons were performed (edgeR, GLM approach for the design matrix setup, the factors were combined together). To obtain reference gene expression profile datasets for native α- and β-cell phenotypes, DEGs between sorted α- and β-cells were analysed (FC > 2 FDR < 0.01). The 2,940 DEGs were used as reference set of genes to separate α- and β-cell-specific expression patterns (1,682 DEGs as α-cell genes, 1,258 DEGs as β-cell genes). Three additional comparisons were generated with respect to the reference α-cells: αDT versus α, αPdx1OE versus α and αPdx1OE + diphtheria toxin versus α (FDR < 0.05). All DEGs we identified are provided in Supplementary Table 2.

We considered upregulated β-cell genes or downregulated α-cell genes in the DEGs list as genes inducing a β-cell signature ('induced β-cell signature' category) and, reciprocally, upregulated α-cell genes as enhancing α-cell signature ('enhanced α-cell signature' category). DEGs from each condition were intersected with α-/β -cell reference genes and shown in Fig. 3b and Supplementary Table 2. The output data were displayed graphically as a principal component analysis-plot, heatmap, dendrogram or Venn diagram.

Pathway analysis. The pathway analyses were performed with gene set enrichment analysis (http://software.broadinstitute.org/gsea/index.jsp). Gene sets with significant enrichment in gene set enrichment analysis were identified among mm_GO of Gene Set Knowledgebase. All significant gene sets are shown in Supplementary Table 2.

Physiological studies. Pancreatic glucagon was measured as previously described[49].

C-peptide measurements and pseudoislets experiments. In vivo glucose challenge tests, islets isolation and FACS sorting of YFP$^+$ cells were performed as described in earlier work[12,13]. The gating strategy used for FACS sorting is provided in Supplementary Fig. 2.

For re-aggregation into pseudoislets, sorted islet cells from 3–8 mice were pooled and seeded on 96-well ultra-low adherent culture plates for 5–7 d (1,000 cells well^{-1}) at 37 °C in a 5% CO_2 incubator, in the following culture medium: Advanced DMEM/F12 (Invitrogen) supplemented with penicillin/streptomycin, 10 mM HEPES (Invitrogen), 2 mM GlutaMAX (Invitrogen), 10% fetal bovine serum, 10 mM nicotinamide (Sigma) and 1 mM *N*-acetyl-L-cysteine (Sigma). The culture medium was changed every second day.

For live imaging of cultured cells, images were captured manually on culture day seven using a Nikon Eclipse TE300 microscope.

To evaluate reprogramming events in pseudoislets, the histology of pseudoislets was examined in cryo-sections as described in earlier work[12,13].

Pseudoislets were hand-picked for each assay replicate and washed by incubation for 1 h at 37 °C in RPMI medium (Invitrogen) and then equilibrated by incubation for 1 h at 37 °C in Krebs Ringer Bicarbonate buffer containing 3 mM glucose (Sigma). The samples were then transferred into fresh Krebs Ringer Bicarbonate buffer containing 3 mM glucose (Low) for 1 h followed by incubation for another hour in Krebs Ringer Bicarbonate buffer containing 20 mM glucose (Hi) at 37 °C. The medium was collected after 1 h of incubation at each glucose concentration and stored at −80 °C for subsequent analyses. Mouse C-peptide concentration was quantified using Mouse C-peptide ELISA kit (Alpco).

Sorted α-cells (90,000–225,000 α-cells from 3–8 mice) were pooled for the three independent cohorts of experiments in each control and α-*Smo*-KO group, and re-aggregated into pseudoislets. In glucose-stimulated C-peptide secretion tests, the maximum number of pseudoislets (90–225 pseudoislets) that we could generate from the pooled α-cells was tested as a cohort and then pseudoislet number normalized C-peptide release.

Transplantations. Islet transplantations under the kidney capsule were performed as described in earlier work[50].

Immunofluorescence. Cryostat sections were 10 µm-thick. The antibodies used were: rabbit and guinea pig anti-Pdx1 (1/5000 and 1/750 respectively; C.W. Wright), rabbit anti-Nkx6.1 (1/800; BCBC), guinea pig anti-porcine insulin (1/400; DAKO), mouse anti-glucagon (1/1000; Sigma), mouse anti-somatostatin (1/200; BCBC) or goat anti-somatostatin (1/200; Santa Cruz), rabbit anti-GFP (1/400; Molecular Probes), mouse anti-mCherry (1/500; Abcam) and goat anti-Ihh (1/50; Santa Cruz). Secondary antibodies were coupled to Alexa 405, 488, 647 (Molecular Probes), Cy3, Cy5 (Jackson Immunoresearch) or TRITC (Southern Biotech). All antibodies are listed in Supplementary Table 4. The sections were examined with a confocal microscope (Leica TCS SPE). In all experiments cells were considered

bihormonal (glucagon$^+$insulin$^+$, somatostatin$^+$insulin$^+$) or co-expressing markers (that is, insulin$^+$YFP$^+$) when one nucleus was clearly surrounded by both hormone/reporter staining.

Statistics and reproducibility. Error bars represent s.e.m. or s.d., as indicated in the figure legends. One representative biological replicate of an experiment is presented in the figures. All experiments were performed three or more times independently under identical or similar conditions, except when indicated in the figure legends. Statistical analyses were performed using the Prism v6.0 software and either unpaired *t*-tests or Mann-Whitney tests were applied for sample comparisons. Glycaemia was measured once on multiple time-points for each animal (Fig. 1c). The RNA-Seq experiment/reaction was performed once (Fig. 3, Supplementary Fig. 3a–c). Quantitative PCRs were performed once, using 3–5 individual biological samples as indicated in the figure legends; each biological sample was run in triplicate (Fig. 4 and Supplementary Figs. 3–5). Immunofluorescence for a particular antibody cocktail was performed once for each mouse with ≥3 cryo-sections/animal being stained at once and analysed (Figs. 2c,g,k,i; 4c,f; 5c; 6c,f and Supplementary Figs. 4b,g,j; 5h,j,k,l). The immunofluorescence reaction was repeated twice for Supplementary Fig. 5b.

Reporting Summary. Further information on research design is available in the Nature Research Reporting Summary linked to this article.

Data availability

The RNA-Seq data generated in this study have been deposited in the NCBI GEO database under accession number GSE109285. Source data for Figs. 1–6 and Supplementary Figs. 1,2,4–6 are provided as Supplementary Table 1 and RNA analyses are provided in Supplementary Table 2. All other data supporting the findings of this study are available from the corresponding author on reasonable request.

References

41. Miyatsuka, T. et al. Persistent expression of PDX-1 in the pancreas causes acinar-to-ductal metaplasia through Stat3 activation. *Genes Dev.* **20**, 1435–1440 (2006).
42. Dietrich, P., Dragatsis, I., Xuan, S., Zeitlin, S. & Efstratiadis, A. Conditional mutagenesis in mice with heat shock promoter-driven *cre* transgenes. *Mamm. Genome* **11**, 196–205 (2000).
43. Bruning, J. C. et al. A muscle-specific insulin receptor knockout exhibits features of the metabolic syndrome of NIDDM without altering glucose tolerance. *Mol. Cell* **2**, 559–569 (1998).
44. Long, F., Zhang, X. M., Karp, S., Yang, Y. & McMahon, A. P. Genetic manipulation of hedgehog signaling in the endochondral skeleton reveals a direct role in the regulation of chondrocyte proliferation. *Development* **128**, 5099–5108 (2001).
45. Chen, S. X. et al. Quantification of factors influencing fluorescent protein expression using RMCE to generate an allelic series in the *ROSA26* locus in mice. *Dis. Model Mech.* **4**, 537–547 (2011).
46. Rodriguez, C. I. et al. High-efficiency deleter mice show that FLPe is an alternative to Cre-*loxP*. *Nat. Genet.* **25**, 139–140 (2000).
47. Russell, M. C., Cowan, R. G., Harman, R. M., Walker, A. L. & Quirk, S. M. The hedgehog signaling pathway in the mouse ovary. *Biol. Reprod.* **77**, 226–236 (2007).
48. Li, Z. et al. Reduced white fat mass in adult mice bearing a truncated Patched 1. *Int. J. Biol. Sci.* **4**, 29–36 (2008).
49. Strom, A. et al. Unique mechanisms of growth regulation and tumor suppression upon Apc inactivation in the pancreas. *Development* **134**, 2719–2725 (2007).
50. Mathe, Z. et al. Tetracycline-regulated expression of VEGF-A in beta cells induces angiogenesis: improvement of engraftment following transplantation. *Cell Transplant.* **15**, 621–636 (2006).

nature research

Corresponding author(s): NCB-C35756B

Reporting Summary

Nature Research wishes to improve the reproducibility of the work that we publish. This form provides structure for consistency and transparency in reporting. For further information on Nature Research policies, see Authors & Referees and the Editorial Policy Checklist.

Statistical parameters

When statistical analyses are reported, confirm that the following items are present in the relevant location (e.g. figure legend, table legend, main text, or Methods section).

n/a	Confirmed	
☐	☒	The exact sample size (*n*) for each experimental group/condition, given as a discrete number and unit of measurement
☐	☒	An indication of whether measurements were taken from distinct samples or whether the same sample was measured repeatedly
☐	☒	The statistical test(s) used AND whether they are one- or two-sided *Only common tests should be described solely by name; describe more complex techniques in the Methods section.*
☐	☒	A description of all covariates tested
☒	☐	A description of any assumptions or corrections, such as tests of normality and adjustment for multiple comparisons
☐	☒	A full description of the statistics including central tendency (e.g. means) or other basic estimates (e.g. regression coefficient) AND variation (e.g. standard deviation) or associated estimates of uncertainty (e.g. confidence intervals)
☐	☒	For null hypothesis testing, the test statistic (e.g. *F*, *t*, *r*) with confidence intervals, effect sizes, degrees of freedom and *P* value noted *Give P values as exact values whenever suitable.*
☒	☐	For Bayesian analysis, information on the choice of priors and Markov chain Monte Carlo settings
☒	☐	For hierarchical and complex designs, identification of the appropriate level for tests and full reporting of outcomes
☒	☐	Estimates of effect sizes (e.g. Cohen's *d*, Pearson's *r*), indicating how they were calculated
☐	☒	Clearly defined error bars *State explicitly what error bars represent (e.g. SD, SE, CI)*

Our web collection on statistics for biologists may be useful.

Software and code

Policy information about availability of computer code

Data collection	CSDiva v 8.0.1 (BD Biosciences) for sorting on a FACSAria2. Summit v 6.2 (Beckman Coulter) for sorting on a Moflo Astrios.
Data analysis	All statistical analyses were performed with GraphPad Prism6. Biological quality control and summarization of RNA samples were done with the RSeQC v2.4, the PicardTools v1.92 and the SamTools v0.1.18. Bioinformatic data were analised with the Ingenuity Pathway Analyses software (Ingenuity Systems, Redwood City, CA). Pathway analyses were performed with gene set enrichment analysis (GSEA, http://software.broadinstitute.org/gsea/index.jsp). Gene sets with significant enrichment in GSEA were identified among mm_GO of Gene Set Knowledgebase (GSKB). The normalization and differential expression analysis was performed with the R/Bioconductor package edgeR package v.3.20.9. For live imaging of cultured cells, images were captured manually at culture day 7 using Nikon Eclipse TE300 microscope (Nikon). Sections were examined with a confocal microscope (Leica TCS SPE). In all experiments cells were manually counted and considered bihormonal (glucagon+insulin+; somatostatin +insulin+) or coexpressing markers (i.e. insulin+YFP+) when one nucleus was clearly surrounded by both hormone / reporter staining.

For manuscripts utilizing custom algorithms or software that are central to the research but not yet described in published literature, software must be made available to editors/reviewers upon request. We strongly encourage code deposition in a community repository (e.g. GitHub). See the Nature Research guidelines for submitting code & software for further information.

Data

Policy information about availability of data

All manuscripts must include a data availability statement. This statement should provide the following information, where applicable:

- Accession codes, unique identifiers, or web links for publicly available datasets
- A list of figures that have associated raw data
- A description of any restrictions on data availability

The RNA-seq data generated in this study have been deposited in the NCBI GEO database under accession number GSE109285. All data and materials used are available from the authors or from commercially available sources.

Field-specific reporting

Please select the best fit for your research. If you are not sure, read the appropriate sections before making your selection.

☒ Life sciences ☐ Behavioural & social sciences ☐ Ecological, evolutionary & environmental sciences

For a reference copy of the document with all sections, see nature.com/authors/policies/ReportingSummary-flat.pdf

Life sciences study design

All studies must disclose on these points even when the disclosure is negative.

Sample size	Sample size was chosen to ensure adequate power and to detect a pre-specified effect based on the available literature and protocols in the field. Therefore, sample sizes are comparable with the ones used in the published literature in the field. For multiple transgenics and transplantation studies the numbers were also limited by the availability of the phenotype. No statistical methods were used to predetermine sample size.
Data exclusions	At the beginning of each experiment, mice must be (1) healthy, (2) normoglycemic, (4) bearing all the desired transgenes, (5) for age-matched controls we prefered, when possible, litter mates. These exclusion criteria were pre-established. For the analyses of the RNA-seq data sonly only one outliner data point was excluded due to incorrect genotyping (false negative).
Replication	For all experiments, all attempts at replication were successful.
Randomization	In the in vivo experiments, between members of the same litter we randomly selected the experimental animals and controls.
Blinding	No blinding was possible during treatment do to regular glycemia control.

Reporting for specific materials, systems and methods

Materials & experimental systems

n/a	Involved in the study
☒	☐ Unique biological materials
☐	☒ Antibodies
☐	☒ Eukaryotic cell lines
☒	☐ Palaeontology
☐	☒ Animals and other organisms
☒	☐ Human research participants

Methods

n/a	Involved in the study
☒	☐ ChIP-seq
☐	☒ Flow cytometry
☒	☐ MRI-based neuroimaging

Antibodies

Antibodies used	Antibodies used in this study are the following: Rabbit and guinea pig anti-Pdx1 (C.W. Wright, 1/5000 and 1/750 respectively), Rabbit anti-Nkx6.1 (BCBC AB1069, 1/800), Guinea pig anti-porcine insulin (DAKO, 1/400), Mouse anti-glucagon (Sigma, 1/1000), Mouse anti-somatostatin (BCBC Ab1985, 1/200) or Goat anti-somatostatin (Santa Cruz 7918 1:200), Rabbit anti-GFP (Molecular Probes, 1/400), Mouse anti-mCherry (Abcam ab125096, 1/500), Goat anti-Ihh (Santa Cruz sc-1196 1:50). Secondary antibodies were coupled to Alexa 405, 488, 647 (Molecular Probes), Cy3, Cy5 (Jackson Immunoresearch), or TRITC (Southern Biotech) and all used at a 1/500 dilution.

Validation	All antibodies used were validated by the respective commercial source for the application used in this manuscript.

Eukaryotic cell lines

Policy information about cell lines

Cell line source(s)	No cell lines were used in the manuscript.
Authentication	The cell lines were not authenticated.
Mycoplasma contamination	The cell lines were not tested for mycoplasma contamination.
Commonly misidentified lines (See ICLAC register)	No cell lines used in this study were found in the database of commonly misidentified cell lines that is maintained by ICLAC and NCBI Biosample.

Animals and other organisms

Policy information about studies involving animals; ARRIVE guidelines recommended for reporting animal research

Laboratory animals	All transgenic mice used in this studies had a mixed background. 2-3 months old male and female mice were used for all experiments, except for transplantation experiments, where only males were used as hosts.
Wild animals	No wild animals were used in this study.
Field-collected samples	No field-collected samples were used in this study.

Flow Cytometry

Plots

Confirm that:

☒ The axis labels state the marker and fluorochrome used (e.g. CD4-FITC).

☒ The axis scales are clearly visible. Include numbers along axes only for bottom left plot of group (a 'group' is an analysis of identical markers).

☒ All plots are contour plots with outliers or pseudocolor plots.

☒ A numerical value for number of cells or percentage (with statistics) is provided.

Methodology

Sample preparation	RNA-Seq analyses, islet isolation and cell isolation by flow cytometry (FACS) were performed using previously described protocols (Chera et al 2014). Purified cells were obtained as follows: - mature α-cells from 3-month-old Glucagon-Venus mice (whose glucagon-expressing α-cells also express the fluorescent reporter Venus). - α-cells 30 days after DT from Glucagon-Venus; RIP-DTR mice (whose glucagon-expressing α-cells express the fluorescent reporter Venus and β-cells can be ablated by DT administration), injected with DT at 2 months of age. - mature β-cells from 3-month-old Insulin-mCherry mice (whose insulin-expressing β-cells also express the fluorescent reporter mCherry). - α-cells ectopically expressing PDX1 from 3-month-old Glucagon-rtTA; TetO-Cre; R26YFP; CAG-Pdx1 (whose glucagon-expressing α-cells express the transcription factor PDX1 and the fluorescent reporter YFP upon DOX administration). 18 - α-cells expressing PDX1 30 days after DT from Glucagon-rtTA; TetO-Cre; R26YFP; CAG-Pdx1; RIP-DTR mice (in which α-cells express PDX1 and YFP after DOX administration, and β-cells can be ablated with DT).
Instrument	Cells were sorted on a FACSAria2 (BD Biosciences) or Moflo Astrios (Beckman Coulter) system.
Software	FACSDiva v 8.0.1 (BD Biosciences) for sorting on a FACSAria2. Summit v 6.2 (Beckman Coulter) for sorting on a Moflo Astrios. Kaluza Analysis v 2.0 (Beckman Coulter) for analysis.
Cell population abundance	For validation of the purity, small fractions of sorted cells were FACS-sorted again to confirm the gating strategy, and also evaluated by immunostaining, showing more than 99% abundance within the post-sort fractions.
Gating strategy	Single viable islet cells were gated by forward scatter, side scatter and pulse-width parameters and by negative staining for DAPI (Life Technologies) or DRAQ7 (B25595, BD Biosciences) to remove doublets and dead cells. Boundaries between positive and negative were very clear because of very high expression of reporter proteins.

☒ Tick this box to confirm that a figure exemplifying the gating strategy is provided in the Supplementary Information.